Chapter 3

3D Tsunami Analysis Model

3.1 Introduction

In this study, the VOF method [8] which is one of the robust interface-capturing methods is introduced. Furthermore, the phase-field model [15],[16] is also introduced to compare with the VOF method.

3.1.1 VOF Method

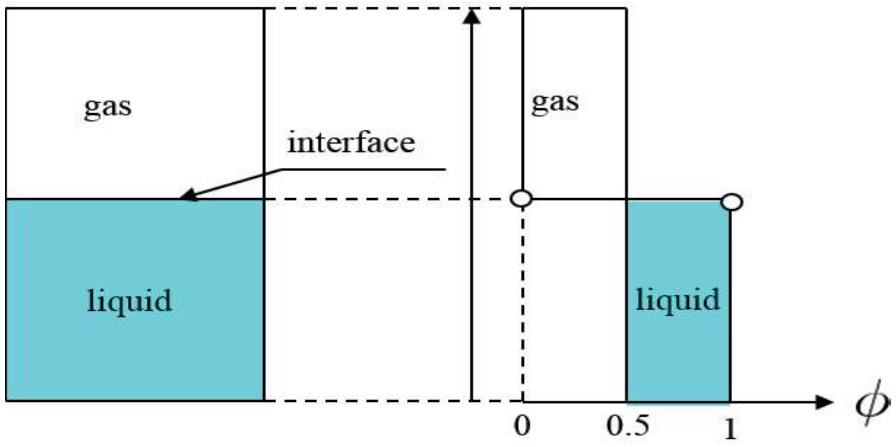

Figure 3.1 **Definition for the color function ϕ of VOF**

The VOF method is an Eulerian method that uses a scalar function ϕ (often referred as a color function) to determine the location of the interface between two different phases in all fixed cells of a computational domain. For the definition of the color

function ϕ, $\phi = 1.0$ indicates the liquid phase, $\phi = 0.0$ indicates the gas phase, $\phi = 0.5$ indicates the interface (see **Figure 3.1**). The advection equation is used as the governing equation of the free surface.

According to the definition, the value of ϕ should vary from 0.0 to 1.0. However, overshoot and undershoot will occur during the computation of ϕ. In that case, the cut-off process is done, for $\phi < 0.0$, ϕ is set to be 0.0, while $\phi > 1.0$, ϕ is set to be 1.0. Therefore, the volume will increase or decrease comparing to the initial volume. What's more, the sharpness of the interface cannot be kept as the computation progressing. To deal with these problems, volume correction method and interface-sharpening technique can be applied.

3.1.2 Phase-Field Model

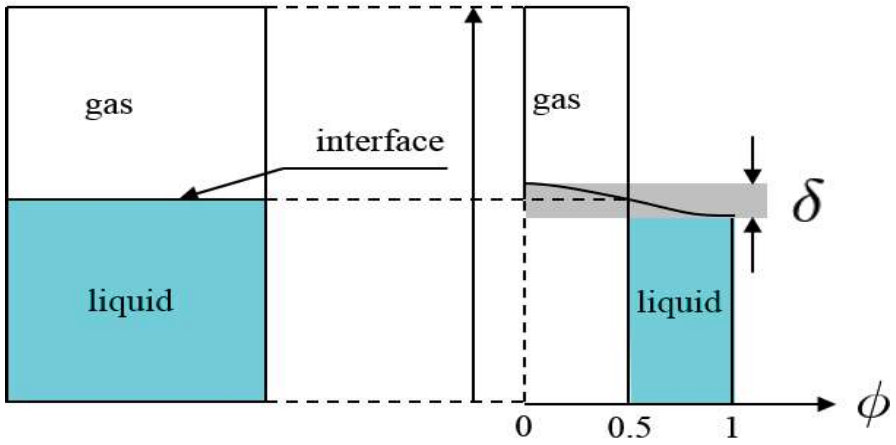

Figure 3.2 **Definition for the color function ϕ of PFM**

The phase-field model PFM [15]-[19] has been widely used to many interfacial problems, such as solidification dynamics problem, fracture dynamics problem, etc. Recently, the PFM is increasingly used for modeling two phase flow. For the PFM, the sharp interface is replaced by thin transition regions where the interfacial forces are smoothly distributed. The definition of the color function is as the same as the VOF method. However, the PFM can keep the width of the interface (see **Figure 3.2**) that can reduce the overshoot and undershoot of the color function. In the PFM, the Allen-Cahn equation [1],[15],[16] or the Cahn-Hilliard equation [1] is normally used as the governing equation. In this study, the Allen-Cahn equation is applied.

3.2 Flowchart of Free Surface Flow in 3D Domain

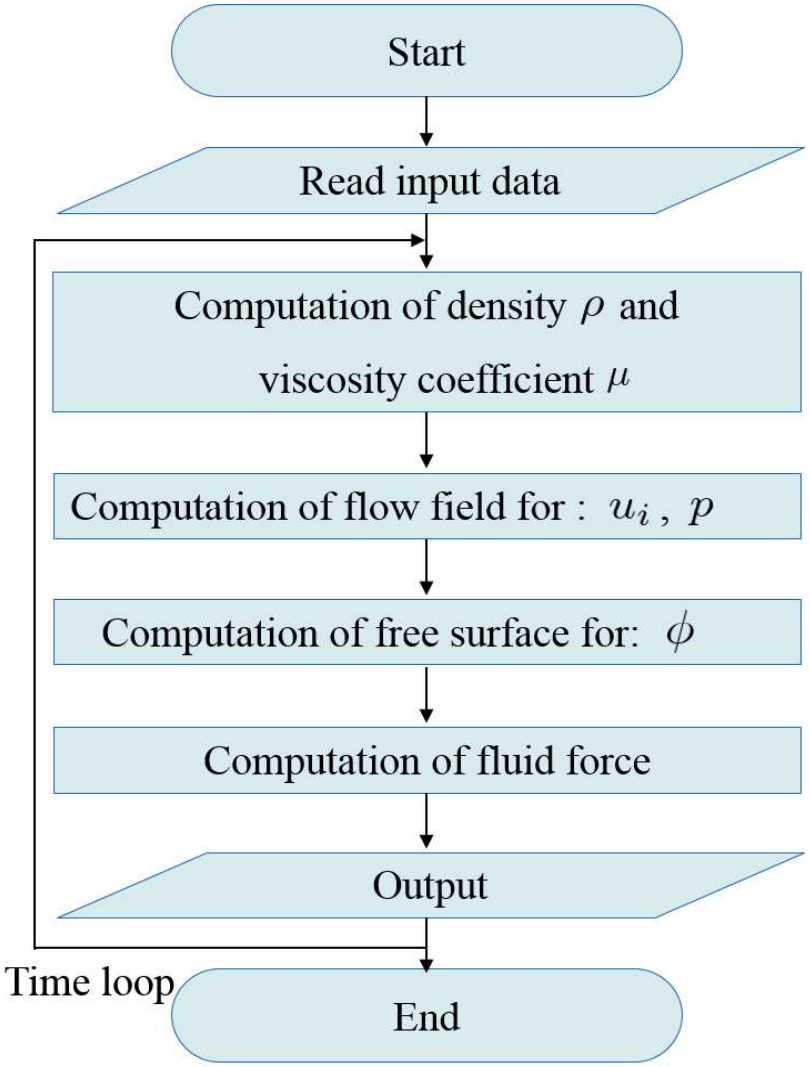

Figure 3.3 **Flowchart of free surface flow in 3D domain**

The flowchart of free surface flow is shown in **Figure 3.3**. Firstly, it reads input data, such as, the mesh, the time increment, the boundary condition, the initial condition, etc. Secondly, it computes the density ρ and the viscosity coefficient μ using the color function. Thirdly, it computes the flow field for the velocity u_i and the pressure p. Fourthly, it computes the free surface for the color function ϕ. Finally, it computes the fluid force if it is needed. The details are introduced in the following sections.

3.3 Computation of Density and Viscosity Coefficients

For the VOF method, the density ρ and viscosity coefficient μ are defined as,

$$\rho = \rho_l \phi + \rho_g (1 - \phi), \tag{3.1}$$

$$\mu = \mu_l \phi + \mu_g (1 - \phi). \tag{3.2}$$

For the phase-field model, the density ρ and viscosity coefficient μ are defined as continuous functions of ϕ [73],[74],[75],

$$\rho = \frac{\rho_l + \rho_g}{2} + \frac{\rho_l - \rho_g}{2} \sin\Big[\frac{\phi - (\phi_l + \phi_g)/2}{\phi_l - \phi_g}\pi\Big], \tag{3.3}$$

$$\mu = \frac{\mu_l + \mu_g}{2} + \frac{\mu_l - \mu_g}{2} \sin\Big[\frac{\phi - (\phi_l + \phi_g)/2}{\phi_l - \phi_g}\pi\Big], \tag{3.4}$$

where $\rho_l, \rho_g, \mu_l, \mu_g$ are density and viscosity coefficient of liquid and gas phases, respectively.

3.4 Computation of Flow Field

3.4.1 Governing Equations of Flow

The incompressible viscous fluid is considered in this study. The Navier-Stokes equations **(3.5)** and the continuity equation **(3.6)** are written as

$$\rho\Big(\frac{\partial u_i}{\partial t}+u_j\frac{\partial u_i}{\partial x_j}-f_i\Big)+\frac{\partial p}{\partial x_i}-\mu\frac{\partial}{\partial x_j}\Big(\frac{\partial u_i}{\partial x_j}+\frac{\partial u_j}{\partial x_i}\Big)=0, \tag{3.5}$$

$$\frac{\partial u_i}{\partial x_i}=0. \tag{3.6}$$

where ρ, u_i, f, p, μ are the density, velocity, body force, pressure, viscosity coefficient, respectively.

The Dirichlet boundary condition and the Neumann boundary are given by

$$u_i=g_i \quad on \quad \Gamma_g, \tag{3.7}$$

$$\Big[-p\delta_{ij}+\mu\Big(\frac{\partial u_i}{\partial x_j}+\frac{\partial u_j}{\partial x_i}\Big)\Big]n_j=h_i \quad on \quad \Gamma_h, \tag{3.8}$$

where n_j is the outward unit normal vector of boundary, Γ_g is Dirichlet boundary (basic boundary), Γ_h is Neumann boundary (natural boundary), g_i, h_i are the flow velocity and traction defined on the boundary. δ_{ij} is the Kronecker's delta.

3.4.2 Spatial Discretization

The governing equations **(3.5)** and **(3.6)** can be discretized by the stabilized finite element method based on the SUPG (Streamline Upwind/Petrov-Galerkin)/PSPG (Pressure Stabilizing/Petrov-Galerkin) method [32],[72]. The following weighted residual equations can be obtained.

$$\begin{aligned}
&\int_\Omega w_i^h\cdot\rho\Big(\frac{\partial u_i^h}{\partial t}+u_j^h\frac{\partial u_i^h}{\partial x_j}-f_i\Big)d\Omega-\int_\Omega\frac{\partial w_i^h}{\partial x_i}p^h d\Omega\\
&+\int_\Omega q^h\frac{\partial u_i^h}{\partial x_i}d\Omega+\int_\Omega\frac{\partial w_i^h}{\partial x_j}\mu\Big(\frac{\partial u_i^h}{\partial x_j}+\frac{\partial u_j^h}{\partial x_i}\Big)d\Omega\\
&+\sum_{e=1}^{n_{el}}\int_\Omega\Big(\tau_{\mathrm{SUPG}}u_j^h\frac{\partial w_i^h}{\partial x_j}+\tau_{\mathrm{PSPG}}\frac{1}{\rho}\frac{\partial q^h}{\partial x_i}\Big)\\
&\cdot\Big\{\rho\Big(\frac{\partial u_i^h}{\partial t}+u_j^h\frac{\partial u_i^h}{\partial x_j}-f_i\Big)+\frac{\partial p_i^h}{\partial x_i}\Big\}d\Omega
\end{aligned}$$

$$+\sum_{e=1}^{n_{el}}\int_{\Omega}\tau_{\mathrm{CONT}}\frac{\partial w_i^h}{\partial x_i}\rho\frac{\partial u_j^h}{\partial x_j}d\Omega$$
$$=\int_{\Gamma_h} w_i^h h_i d\Gamma_h, \tag{3.9}$$

where w_i, q are the weight functions of flow velocity and pressure, and n_{el} is the number of elements. The first to the fourth terms are the Galerkin terms, the fifth term is the SUPG term, the sixth term is the PSPG term, the seventh term is the shock-capturing term. τ_{SUPG}, τ_{PSPG}, τ_{CONT} are the stabilized parameters, they are decided by the following equations,

$$\tau_{\mathrm{SUPG}}=\left\{\left(\frac{2}{\Delta t}\right)^2+\left(\frac{2\parallel u_i^h\parallel}{h_e}\right)^2+\left(\frac{4\nu}{h_e^2}\right)^2\right\}^{-\frac{1}{2}}, \tag{3.10}$$

$$\tau_{\mathrm{SUPG}}=\tau_{\mathrm{PSPG}}, \tag{3.11}$$

$$\tau_{\mathrm{CONT}}=\frac{h_e}{2}\parallel u_i^h\parallel z(\mathrm{Re}_u), \tag{3.12}$$

where ν is kinematic viscosity coefficient. h_e is the element size decided by the following equation,

$$h_e=2\left(\sum_{e=1}^{n_{en}} s_i\cdot N_{\alpha,i}\right)^{-1}, \tag{3.13}$$

where n_{en} is the number of nodes of an element, s_i is the unit normal vector of flow velocity. N_α is the shape function. Re_u is the Reynolds number and z is denoted as,

$$z(\mathrm{Re}_u)=z\left(\frac{\parallel u_i^h\parallel h_e}{2\nu}\right)=\begin{cases}\frac{\mathrm{Re}_u}{3} & 0\leq\mathrm{Re}_u\leq 3,\\ 1 & 3<\mathrm{Re}_u.\end{cases} \tag{3.14}$$

To apply the first order P1/P1 element with velocity and pressure for the equation **(3.9)**, the following equations can be derived,

$$(\mathbf{M}+\mathbf{M}_{\mathrm{S}})\frac{du_i}{dt}+(\mathbf{A}+\mathbf{A}_{\mathrm{S}})u_i-(\mathbf{G}_i-\mathbf{G}_{\mathrm{S}i})p$$
$$+\mathbf{D}_{ij}u_j+\mathbf{S}_{ij}u_j=(\mathbf{F}+\mathbf{F}_{\mathrm{S}})f_i, \tag{3.15}$$

$$\mathbf{C}_j u_j+\mathbf{M}_{\mathrm{p}j}\frac{du_j}{dt}+\mathbf{A}_{\mathrm{p}j}u_j+\mathbf{G}_{\mathrm{p}}p=\mathbf{F}_{\mathrm{p}}f_i, \tag{3.16}$$

where u is flow velocity, p is pressure. $\mathbf{M}$, $\mathbf{A}$, $\mathbf{G}$, $\mathbf{D}$, $\mathbf{S}$, $\mathbf{F}$, $\mathbf{C}$ are coefficient matrices for each term of time, advection, pressure, viscosity, shock-capturing, body force, continuity. Matrices with subscript of S and P indicate them caused by SUPG and PSPG method.

3.4.3 Temporal Discretization

The time derivative term can be written as,

$$\frac{du_i}{dt} = \frac{u_i^{n+1} - u_i^n}{\Delta t}. \tag{3.17}$$

The Crank-Nicolson method with second order accuracy is applied for the velocity, the pressure is treated implicitly for Eqs. **(3.15)**, **(3.16)**, the following equations can be obtained,

$$\begin{aligned}&(\mathbf{M} + \mathbf{M}_{\mathrm{S}})\frac{u_i^{n+1} - u_i^n}{\Delta t} + (\mathbf{A} + \mathbf{A}_{\mathrm{S}})u_i^{n+\frac{1}{2}} - (\mathbf{G}_i - \mathbf{G}_{\mathrm{S}i})p^{n+1} \\ &+ \mathbf{D}_{ij}u_j^{n+\frac{1}{2}} + \mathbf{S}_{ij}u_j^{n+\frac{1}{2}} = (\mathbf{F} + \mathbf{F}_{\mathrm{S}})f_i,\end{aligned} \tag{3.18}$$

$$\mathbf{C}_j u_j^{n+1} + \mathbf{M}_{\mathrm{p}j}\frac{u_i^{n+1} - u_i^n}{\Delta t} + \mathbf{A}_{\mathrm{p}j}u_j^{n+\frac{1}{2}} + \mathbf{G}_{\mathrm{p}}p^{n+1} = \mathbf{F}_{\mathrm{p}}f_i, \tag{3.19}$$

where $u_i^{n+\frac{1}{2}}$ is defined as

$$u_i^{n+\frac{1}{2}} = \frac{1}{2}(u_i^{n+1} + u_i^n), \tag{3.20}$$

the advection velocity u_j is approximated by the Adams-Bashforth method with a second order accuracy. u_j is defined as the following linearized equation,

$$u_j = \frac{3}{2}u_i^n - \frac{1}{2}u_i^{n-1}. \tag{3.21}$$

Then set the discretized equations **(3.18)**, **(3.19)** by taking the unknown quantity to left and the known quantity to right, and writing into matrix, we can get,

$$\begin{bmatrix} \mathbf{A}_{11} & \mathbf{A}_{12} & \mathbf{A}_{13} & \mathbf{A}_{14} \\ \mathbf{A}_{21} & \mathbf{A}_{22} & \mathbf{A}_{23} & \mathbf{A}_{24} \\ \mathbf{A}_{31} & \mathbf{A}_{32} & \mathbf{A}_{33} & \mathbf{A}_{34} \\ \mathbf{A}_{41} & \mathbf{A}_{42} & \mathbf{A}_{43} & \mathbf{A}_{44} \end{bmatrix} \begin{bmatrix} \mathbf{U}^{n+1} \\ \mathbf{V}^{n+1} \\ \mathbf{W}^{n+1} \\ \mathbf{P}^{n+1} \end{bmatrix} = \begin{bmatrix} \mathbf{b}_1 \\ \mathbf{b}_2 \\ \mathbf{b}_3 \\ \mathbf{b}_4 \end{bmatrix}. \tag{3.22}$$

To solve the simultaneous linear equations **(3.22)**, the element-by-element Bi-CGSTAB (Bi-Conjugate Gradient STABilized) method is applied, the unknown quantities $\mathbf{U^{n+1}}$, $\mathbf{V^{n+1}}$, $\mathbf{W^{n+1}}$, $\mathbf{P^{n+1}}$ can be computed.

3.5 Computation of Free Surface

3.5.1 Governing Equations for Free Surface

For the VOF method, the following advection equation is used as the governing equation for computing free surface,

$$\frac{\partial \phi}{\partial t} + u_j \frac{\partial \phi}{\partial x_j} = 0. \tag{3.23}$$

For the phase-field model, the following Allen-Cahn equation [1],[15],[16] is employed,

$$\frac{\partial \phi}{\partial t} + u_j \frac{\partial \phi}{\partial x_j} = -M_a[\xi(\phi) - k_\phi(\frac{\partial^2 \phi}{\partial x_j^2} + \kappa \Big| \frac{\partial \phi}{\partial x_k} \Big|)], \tag{3.24}$$

where u_j is the advection velocity computed from flow field. ϕ is the color function, $\phi = 1$ denotes fluid, $\phi = 0$ denotes gas, $\phi = 0.5$ denotes free surface. M_a, $\xi(\phi)$, k_ϕ, κ are defined as,

$$M_a = \frac{2b^2}{\delta^2} M\gamma, \; b = 2tanh^{-1}(1 - 2\lambda), \; \delta = a_\delta h_\delta, \tag{3.25}$$

$$\xi(\phi) = \frac{\partial f(\phi)}{\partial \phi}, \; f(\phi) = \phi^2(1 - \phi)^2, \tag{3.26}$$

$$k_\phi = \frac{\delta^2}{2b^2}, \tag{3.27}$$

$$\kappa = \nabla \cdot \mathbf{n}, \; \mathbf{n} = \frac{\nabla \phi}{|\nabla \phi|}, \tag{3.28}$$

where M, γ, δ, h_δ, κ, $\mathbf{n}$ are interface mobility, interface energy, continuously changing gas-liquid interface width, representative length of element, interface curvature, interface normal vector.

3.5.2 Spatial Discretization

Applying the stabilized finite element method based on the SUPG method to Eq. **(3.23)**, the following weighted residual equations can be obtained,

$$\begin{aligned}&\int_\Omega \psi_i^h \frac{\partial \phi^h}{\partial t} d\Omega + \int_\Omega \psi_i^h u_i \frac{\partial \phi^h}{\partial x_i} d\Omega \\ &+ \sum_{e=1}^{n_{el}} \int_{\Omega_e} \tau_{\mathrm{SUPG}} u_i \frac{\partial \psi^h}{\partial x_i} \Big(\frac{\partial \phi^h}{\partial t} + u_j \frac{\partial \phi^h}{\partial x_j} \Big) d\Omega \\ &+ \sum_{e=1}^{n_{el}} \int_{\Omega_e} \tau_{\mathrm{LSIC}} \frac{\partial \psi^h}{\partial x_i} \frac{\partial \phi^h}{\partial x_i} d\Omega = 0, \end{aligned} \tag{3.29}$$

where ψ^h is the weight function for ϕ, τ_{SUPG}, τ_{LSIC} are the stabilized parameter for the SUPG term and the shock capturing term defined as,

$$\tau_{\mathrm{SUPG}} = \Big[\Big(\frac{2}{\Delta t} \Big)^2 + \Big(\frac{2||u_i^e||}{h_e} \Big) \Big]^{-\frac{1}{2}}, \tag{3.30}$$

$$\tau_{\mathrm{LSIC}} = \frac{h_e}{2} ||u_i^e||. \tag{3.31}$$

Applying the stabilized finite element method based on the SUPG method to Eq. **(3.24)**, the following weighted residual equations can be obtained,

$$\begin{aligned}&\int_\Omega \psi^* \Big(\frac{\partial \phi}{\partial t} + u_j \frac{\partial \phi}{\partial x_j} + M_a \xi(\phi) - M_a k_\phi \kappa \Big| \frac{\partial \phi}{\partial x_k} \Big| \Big) d\Omega \\ &- \int_\Omega \psi^* M_a k_\phi \frac{\partial^2 \phi}{\partial x_j^2} d\Omega + \sum_{e=1}^{n_{el}} \int_\Omega \tau_{\mathrm{SUPG}} u_j \frac{\partial \psi^*}{\partial x_j} \Big(\frac{\partial \phi}{\partial t} \\ &+ u_j \frac{\partial \phi}{\partial x_j} + M_a \xi(\phi) - M_a k_\phi \kappa \Big| \frac{\partial \phi}{\partial x_k} \Big| \Big) d\Omega = 0, \end{aligned} \tag{3.32}$$

where ψ^* is the weight function for ϕ.

Using the first order tetrahedron element to make interpolation for Eq. **(3.29)**, the following equations can be derived,

$$(\mathbf{M} + \mathbf{M}_{\mathrm{S}}) \frac{d\phi}{dt} + (\mathbf{A} + \mathbf{A}_{\mathrm{S}} + \mathbf{S}) \phi = 0. \tag{3.33}$$

For the Eq. **(3.32)**, one can get,

$$(\mathbf{M} + \mathbf{M_s}) \frac{d\phi}{dt} + (\mathbf{A} + \mathbf{A_s}) \phi + (\mathbf{M} + \mathbf{M_s}) M_a \xi(\phi) + \mathbf{K}\phi - (\mathbf{M} + \mathbf{M_s}) M_a k_\phi \kappa \Big| \frac{\partial \phi}{\partial x_k} \Big| = 0. \tag{3.34}$$

3.5.3 Temporal Discretization

For the temporal discretization, the following equations are applied.

$$\frac{d\phi}{dt} = \frac{\phi^{n+1} - \phi^n}{\Delta t}, \tag{3.35}$$

$$\phi^{n+\frac{1}{2}} = \frac{1}{2}(\phi^{n+1} + \phi^n). \tag{3.36}$$

To substitute Eqs. **(3.35)** and **(3.36)** into Eqs. **(3.33)** and **(3.34)**, the following equations can be derived,

$$\frac{1}{\Delta t}(\mathbf{M} + \mathbf{M}_\mathrm{S})\phi^{\mathbf{n+1}} + \frac{\mathbf{1}}{\mathbf{2}}(\mathbf{A} + \mathbf{A}_\mathrm{S} + \mathbf{L})\phi^{\mathbf{n+1}} = \frac{\mathbf{1}}{\mathbf{\Delta t}}(\mathbf{M} + \mathbf{M}_\mathrm{S})\phi^{\mathbf{n}} - \frac{\mathbf{1}}{\mathbf{2}}(\mathbf{A} + \mathbf{A}_\mathrm{S} + \mathbf{L})\phi^{\mathbf{n}}, \tag{3.37}$$

$$\begin{aligned}
&\frac{1}{\Delta t}(\mathbf{M} + \mathbf{M_s})\phi^{n+1} + \frac{1}{2}(\mathbf{A} + \mathbf{A_s})\phi^{n+1} + \frac{1}{2}\mathbf{K}\phi^{n+1} \\
&= \frac{1}{\Delta t}(\mathbf{M} + \mathbf{M_s})\phi^{n} - \frac{1}{2}(\mathbf{A} + \mathbf{A_s})\phi^{n} - \frac{1}{2}\mathbf{K}\phi^{n} - (\mathbf{M} + \mathbf{M_s})M_a\xi(\phi^{n+1}) \\
&+ (\mathbf{M} + \mathbf{M_s})M_a k_\phi \kappa^{n+1}\left|\frac{\partial \phi^{n+1}}{\partial x_k}\right|.
\end{aligned} \tag{3.38}$$

To solve the simultaneous linear Eqs. **(3.37)** and **(3.38)**, the diagonal scaling preprocessing method, the element-by-element processing, and the Bi-CGSTAB (Bi-Conjugate Gradient STABilized) method are applied.

3.6 Computation of Fluid Force

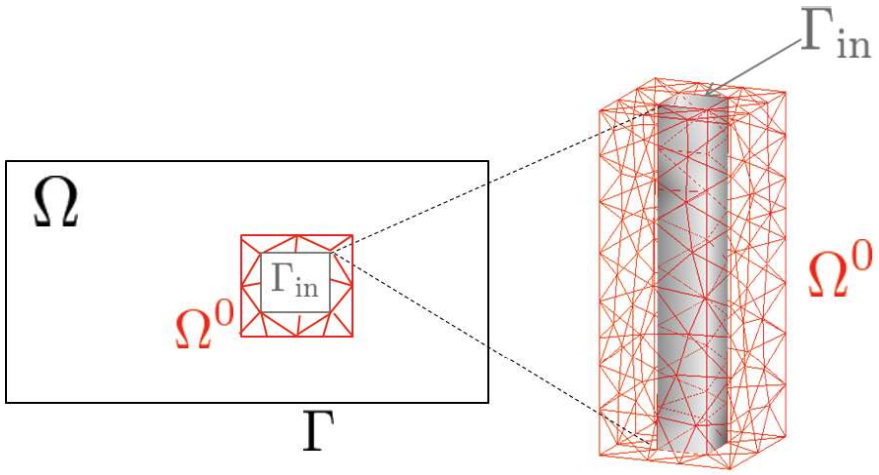

Figure 3.4 **Computational domain of the drag force**

The fluid force which is the drag force by structure is computed by the boundary integral term of the weak formulation derived from Eqs. **(3.5)** and **(3.6)**. For the region Ω^0 which is constituted by the one layer of mesh around the structure in **Figure 3.4**, the drag force can be computed by the following equations [48],

$$\begin{aligned}
&\int_{\Omega^0} w_i^h \cdot \rho\Big(\frac{\partial u_i^h}{\partial t} + u_j^h \frac{\partial u_i^h}{\partial x_j} - f_i\Big) d\Omega - \int_{\Omega^0} \frac{\partial w_i^h}{\partial x_i} p^h d\Omega \\
&+ \int_{\Omega^0} q^h \frac{\partial u_i^h}{\partial x_i} d\Omega + \int_{\Omega^0} \frac{\partial w_i^h}{\partial x_j} \mu\Big(\frac{\partial u_i^h}{\partial x_j} + \frac{\partial u_j^h}{\partial x_i}\Big) d\Omega \\
&= \int_{\Gamma_{in}} w_i^h t_i d\Gamma,
\end{aligned} \tag{3.39}$$

where w_i^h and q^h are weight functions. Γ_{in} is the boundary of structure. To substitute the velocity and the pressure computed from the flow field into the left of Eq. **(3.39)**, the drag force of structure can be computed.

3.7 Volume Correction Method

For the free surface flow, there are many volume correction methods have been proposed, such as the interface-sharpening/mass-conservation method [76], the Yabe and Xiao's method [10]. In this study, the volume correction method proposed by Sakuraba *et al.* [79] is applied. In this method, the color function is corrected near the interface. The volume is corrected by the following steps.

Firstly, to compute the judgment function **(3.40)** and to find the nodes near the interface.

$$D(\phi) = 1 + \cos[2\pi(\phi - 0.5)], \tag{3.40}$$

As shown in **Figure 3.5**, for the interface $D(\phi)$=2, as the phase far from the interface, $D(\phi)$ becomes smaller gradually.

Secondly, the volume $A(t)$ of the nodes near the interface is computed by Eq. **(3.41)**,

$$A(t) = \int_{\Omega} D(\phi) d\Omega. \tag{3.41}$$

Thirdly, the volume error ratio ϕ_{err} is computed by the following equation,

$$\phi_{\mathrm{err}} = \frac{V_{\mathrm{err}}(t)}{A(t)} = \frac{V(t) - V_{\mathrm{init}}}{A(t)}, \tag{3.42}$$

where V_{err}, $V(t)$, V_{init} are the volume error, the volume at t and the initial volume.

Fourthly, to correct the volume by the following two cases using Eq. **(3.43)**. (see **Figure 3.6**)

- Case A ($\phi_{\mathrm{err}} > 0$): in this case, the volume of fluid increases, the volume of the nodes that $0 < \phi < 0.5$ is corrected.
- Case B ($\phi_{\mathrm{err}} \leq 0$): in this case, the volume of fluid decreases, the volume of the nodes that $0.5 \leq \phi < 1$ is corrected.

$$\phi(t) = \phi(t) - 2\phi_{\mathrm{err}} = \begin{cases} 0 < \phi < 0.5, & \phi_{\mathrm{err}} > 0, \\ 0.5 \leq \phi < 1, & \phi_{\mathrm{err}} \leq 0. \end{cases} \tag{3.43}$$

Finally, for $\phi > 1$ and $\phi < 1$, the over amount is cut.

For the problems without inflow and outflow, it is easy to apply the above volume correction method. However, for the 2D-3D hybrid model, the volume of the water in a 3D region is changing because of the inflow and outflow, the volume correction method is not used in this study.

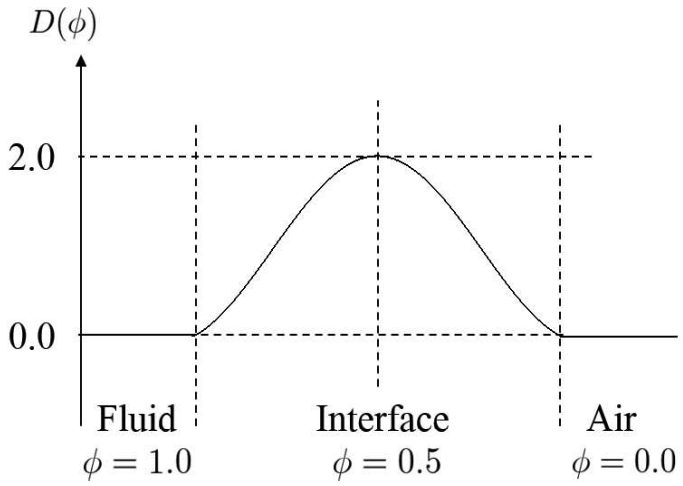

Figure 3.5 **Judgment function of interface**

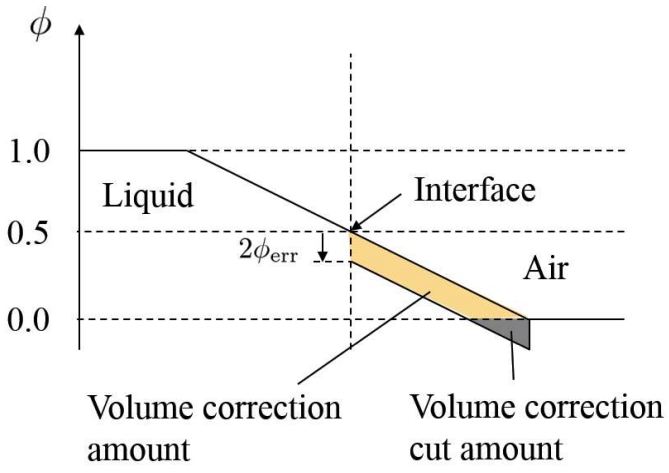

(A) Volume of fluid increase ($\phi_{\mathrm{err}} > 0.0$)

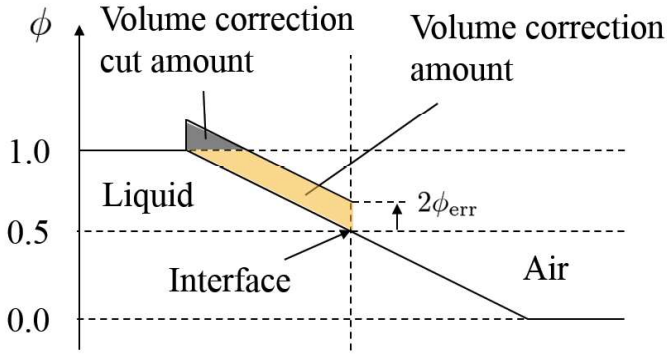

(B) Volume of fluid decrease ($\phi_{\mathrm{err}} < 0.0$)

Figure 3.6 **Conceptual diagram of the volume correction method**

3.8 Numerical Examples

3.8.1 Rotating Cylinder Problem

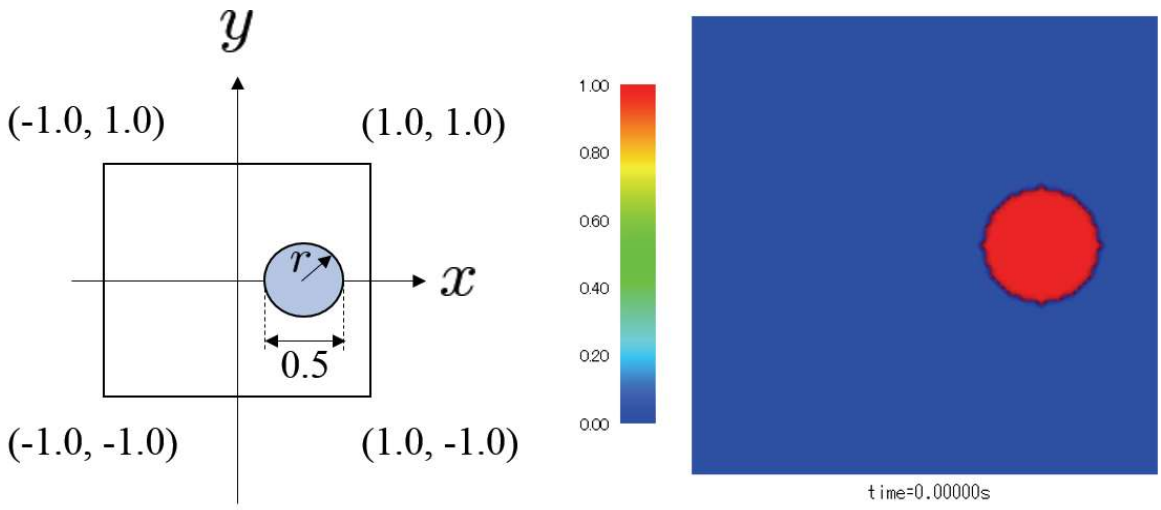

Figure 3.7 **Rotating cylinder problem**

To examine the effectiveness of the PFM based on the Allen-Cahn equation, we simulated a rotating cylinder problem showed in **Figure 3.7**. A comparison to the VOF method based on the advection equation is made. The initial condition is set as $\phi = 1$ $(r \leq 0.25)$, $\phi = 0$ $(r > 0.25)$, and $r^2 = (x - 0.5)^2 + y^2$. The advection velocity is set as $u_j = (-y, x)$. For the computational condition, the mesh size is $\Delta x = \Delta y = 1/48$, the time increment is $\Delta t = \pi/400$. The parameters of the PFM are set as $a_\delta = 3.0$, $\gamma = 0.0001$ for the comparison with the VOF method. Furthermore, in order to investigate the effects of a_δ and γ, comparisons are made by changing the values of a_δ and γ.

Figure 3.8 and **Figure 3.9** show the results after one cycle rotation. The overshoot and undershoot are observed in the results of the VOF method, while they can be reduced by the PFM. And the results by the PFM keep the cylinder better agree to the initial condition than the VOF method. **Figure 3.10**, **Figure 3.11** show the comparisons for the a_δ when $\gamma = 0.0001$. We can see when the value of a_δ increases, the width of the interface becomes larger, but when the $a_\delta = 1$, the shape of cylinder

deforms. From **Figure 3.11**, we can see the results of a_δ =2, 3 are close to the initial shape. **Figure 3.12** and **Figure 3.13** show the comparisons for the γ when $a_\delta = 3.0$, we can see the cylinder becomes smaller when the value of γ increases. From **Figure 3.13**, when $\gamma = 0.005$ the shape of the cylinder deforms much smaller than the initial shape, and the result of $\gamma = 0.0001$ is the most agree to the initial shape. We should note that when $\gamma = 0.0$, the Allen-Cahn equation will become into the advection equation, which will result in overshoot and undershoot.

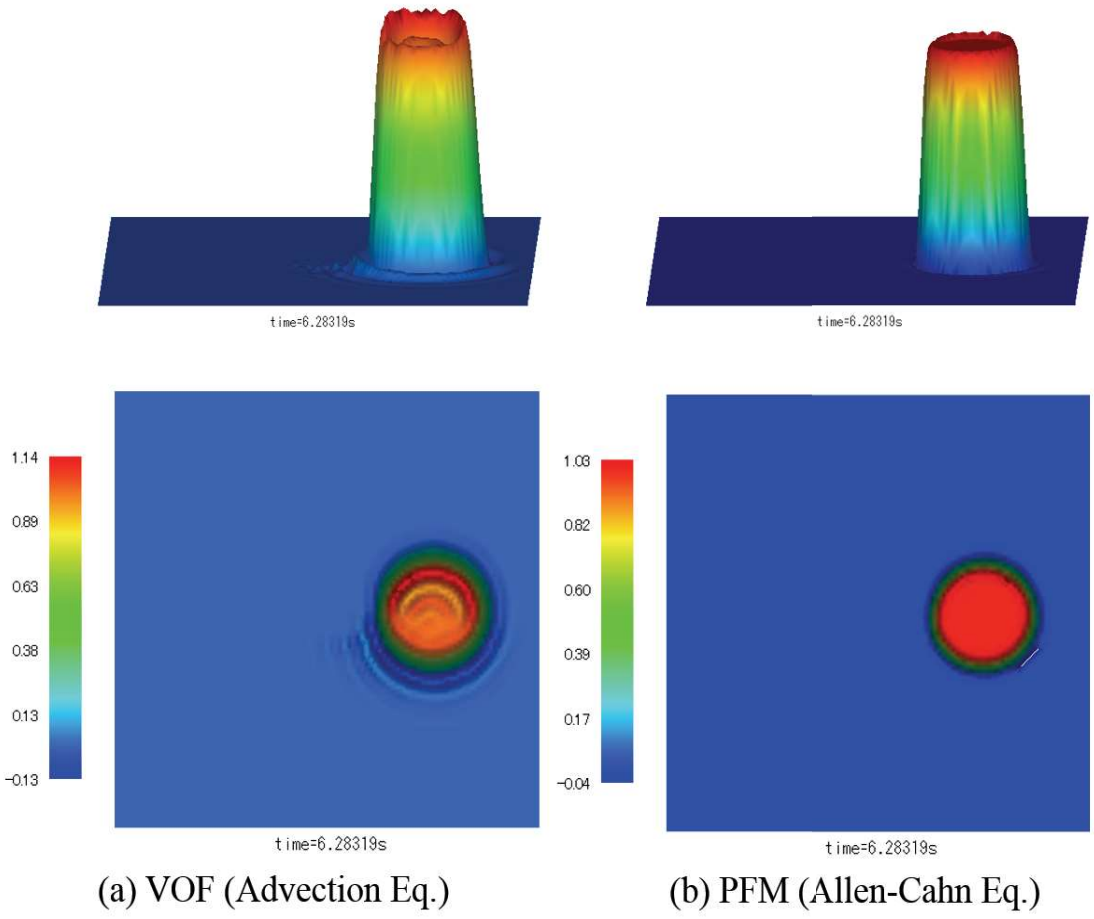

Figure 3.8 **Computational results (after one cycle rotation)**

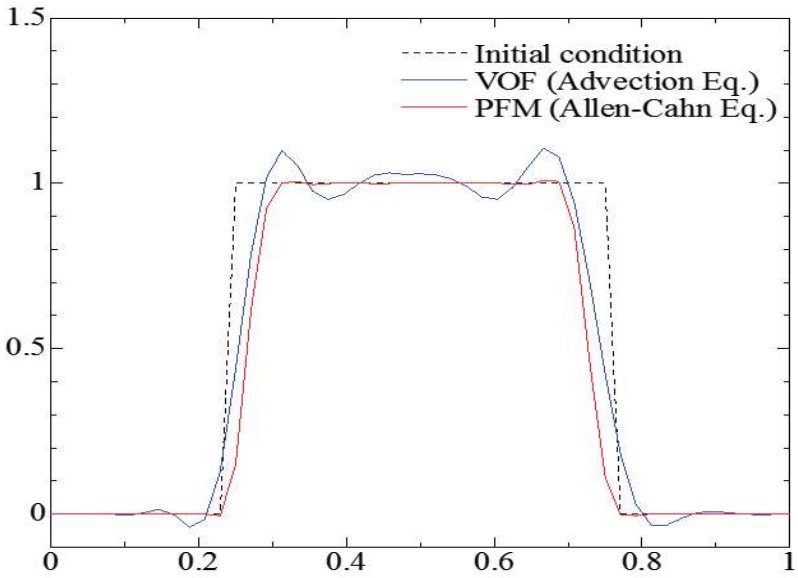

Figure 3.9 **Cross section at y=0**

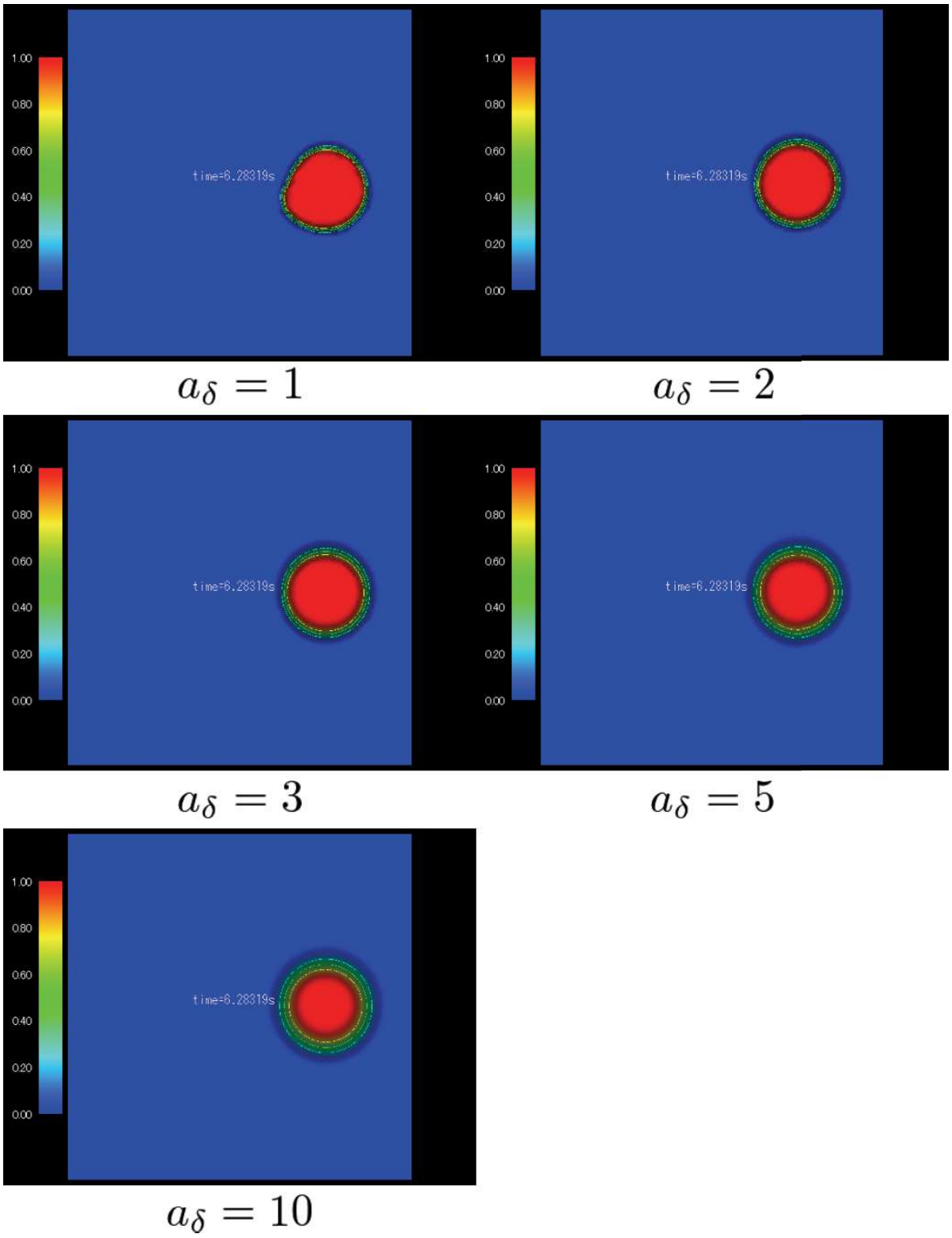

Figure 3.10 **Comparison by changing a_δ ($\gamma = 0.0001$)**

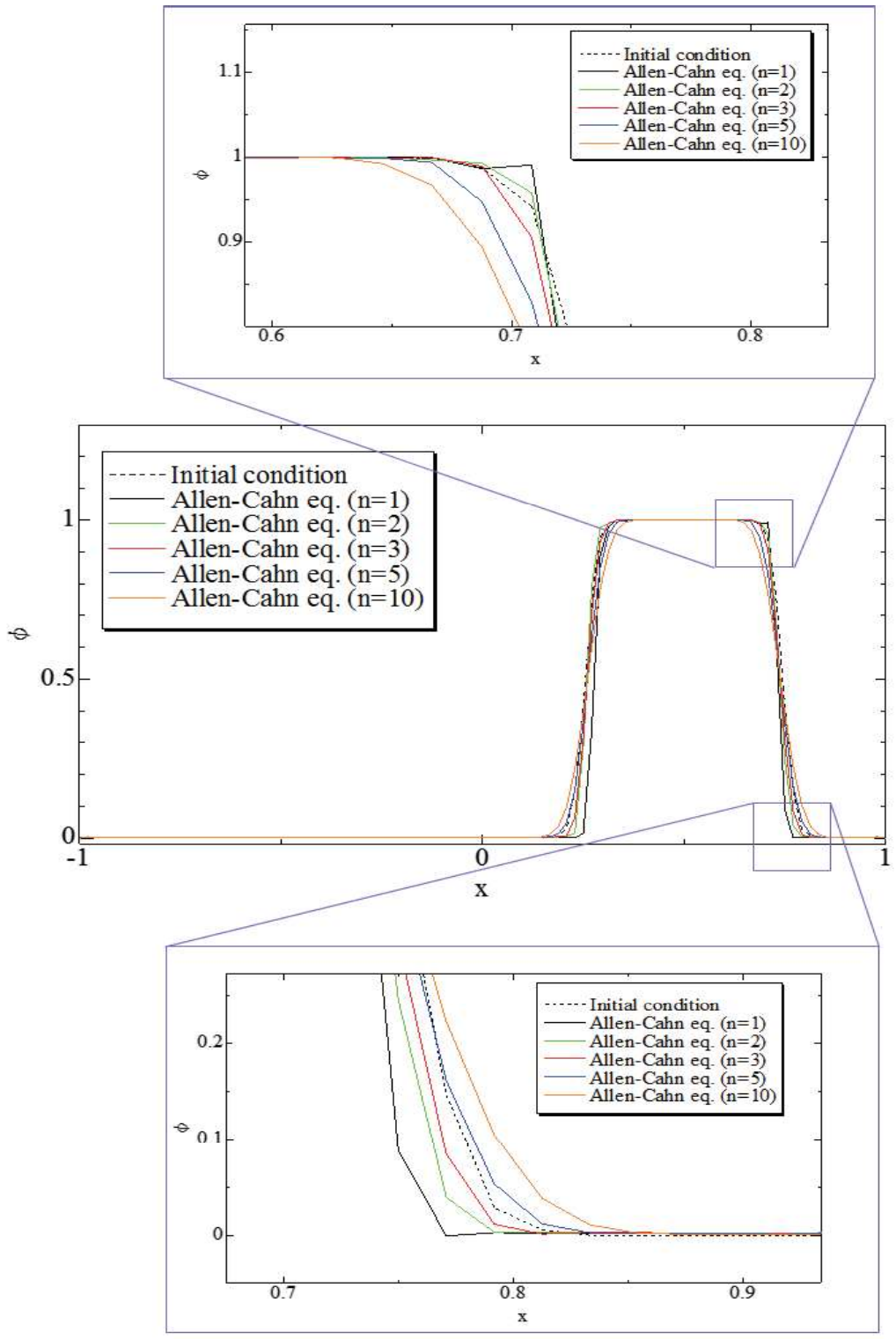

Figure 3.11 **Cross section at y=0** ($\gamma = 0.0001$, $n = a_\delta$)

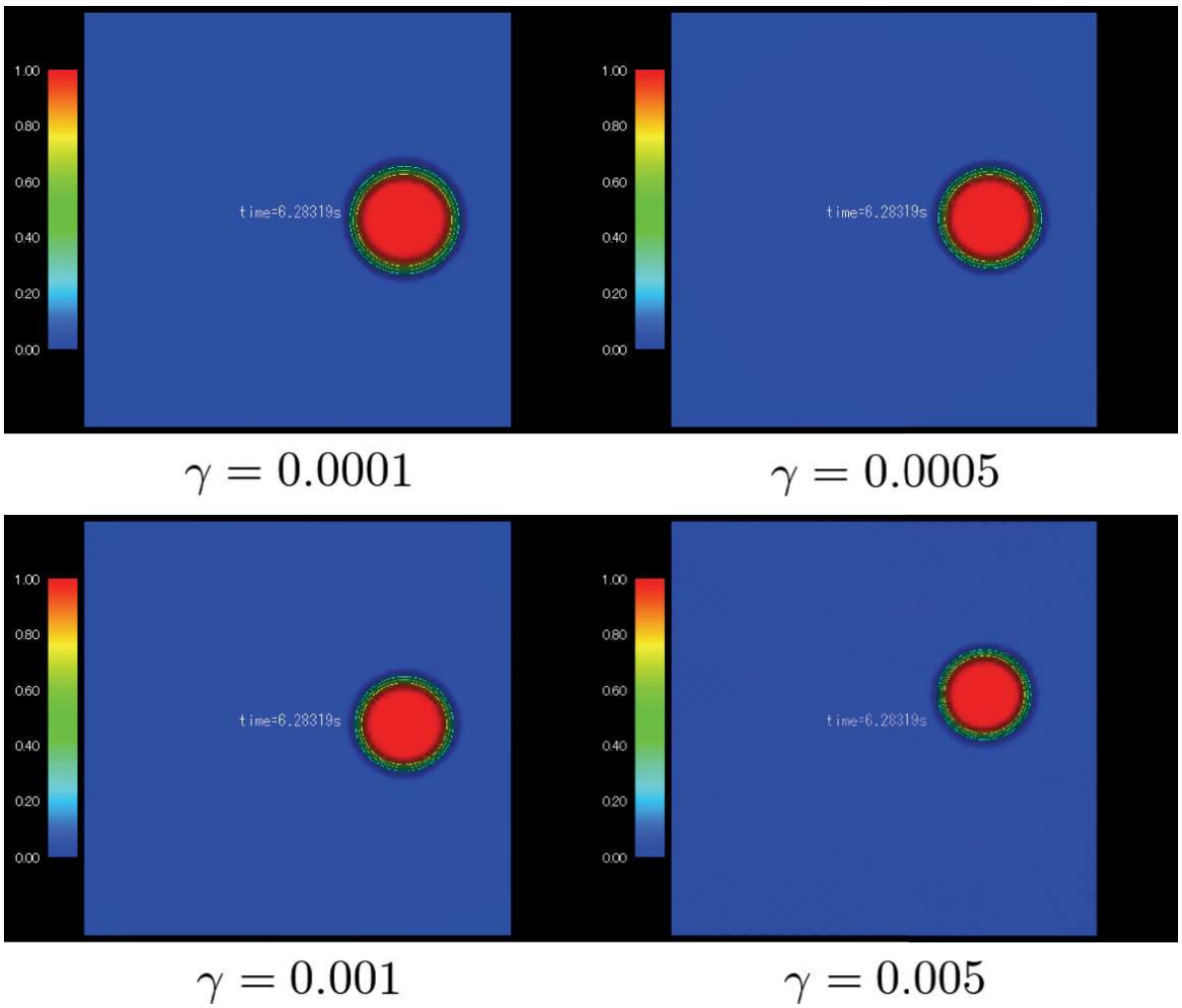

Figure 3.12 **Comparison by changing γ ($a_\delta = 3.0$)**

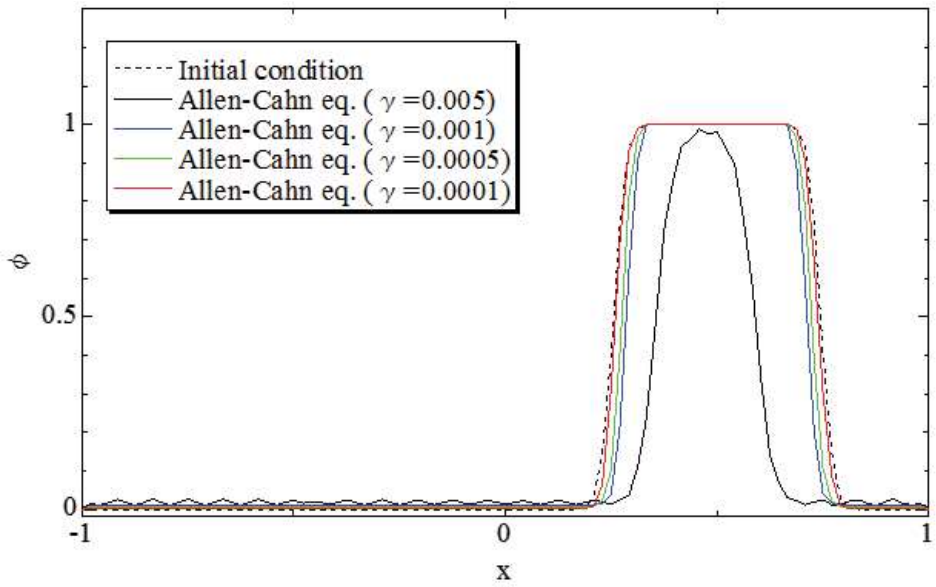

Figure 3.13 **Cross section at y=0 ($a_\delta = 3.0$)**

3.8.2 Dambreak Problem (2D)

In order to test the effectiveness of the PFM by combining with the Navier-Stokes equations, a benchmark problem for free surface flow is simulated (i.e. a dambreak problem showed in **Figure 3.14**). The experimental results [77] and the results by using the VOF method are used for comparison. For this test, a structural grid with 100×75 divisions is used (see **Figure 3.15**). The number of nodes is 7,676 and the number of elements is 15,000. The time increment is set to be 0.001s. The slip condition is set on the walls of the tank. The parameters for the PFM are set as $a_\delta = 2.0$ and $\gamma = 0.001$.

Figure 3.16 shows the snapshots of free surface at t=0.01s, 0.20s, and 1.00s. We can see the thickness of interface by the VOF method becomes wider and the water diffusing into air. However, the thickness of interface is kept almost the same and stable by the PFM. From **Figure 3.17**, we can see the water propagates faster by using the VOF method, because the thickness of interface becomes wider. From **Figure 3.18**, we can see the PFM can conserve the volume better than the VOF method.

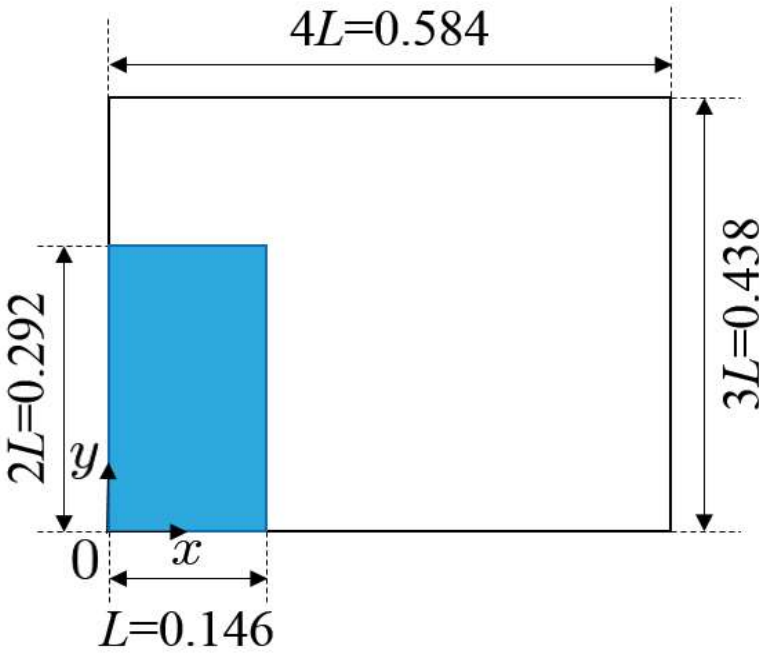

Figure 3.14 **Dambreak problem**

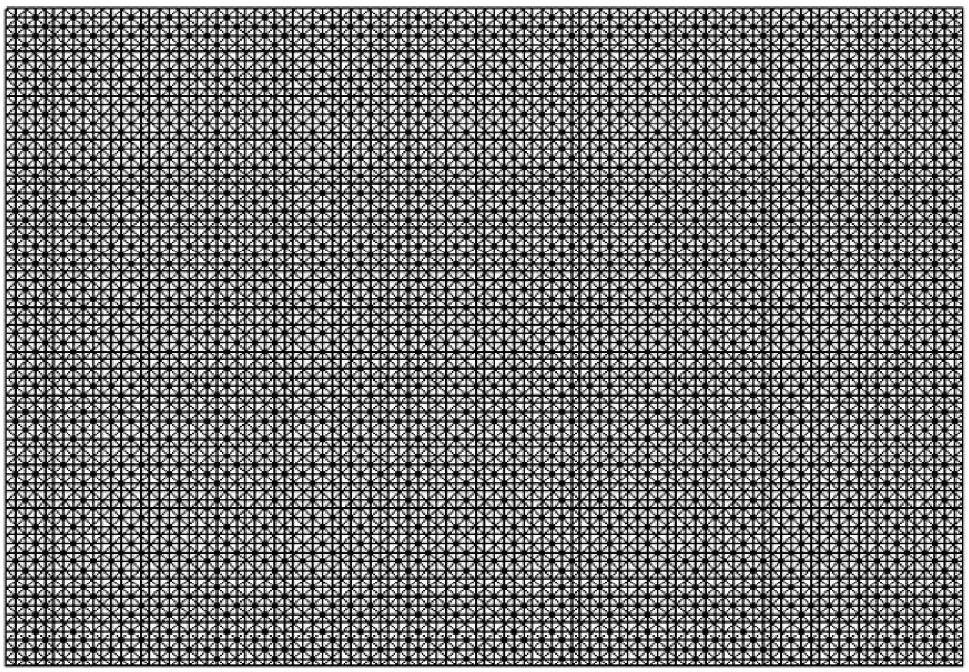

Figure 3.15 **Computational mesh for dambreak problem**

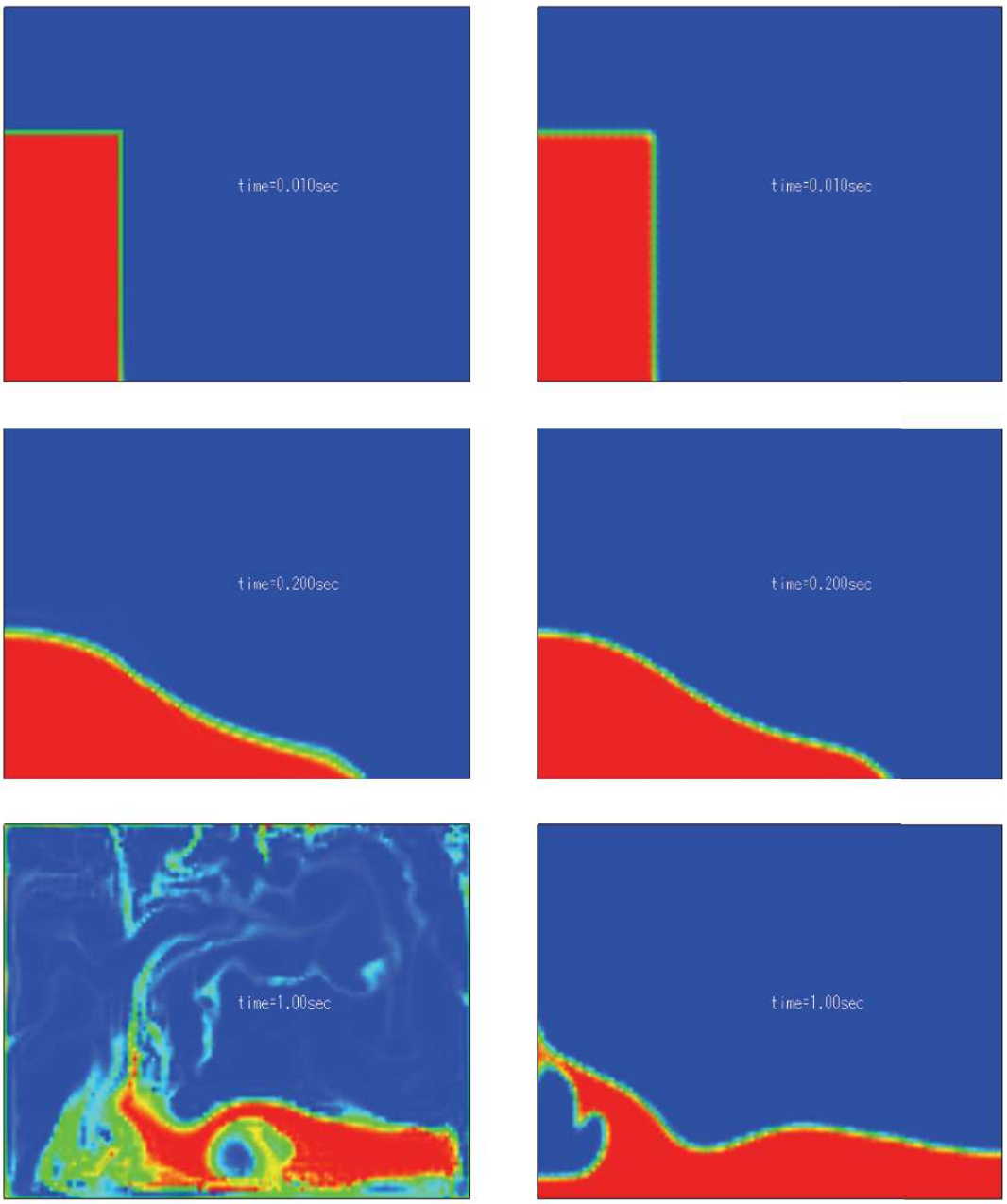

Figure 3.16 **Snapshots at t=0.01s, 0.20s, and 1.00s**

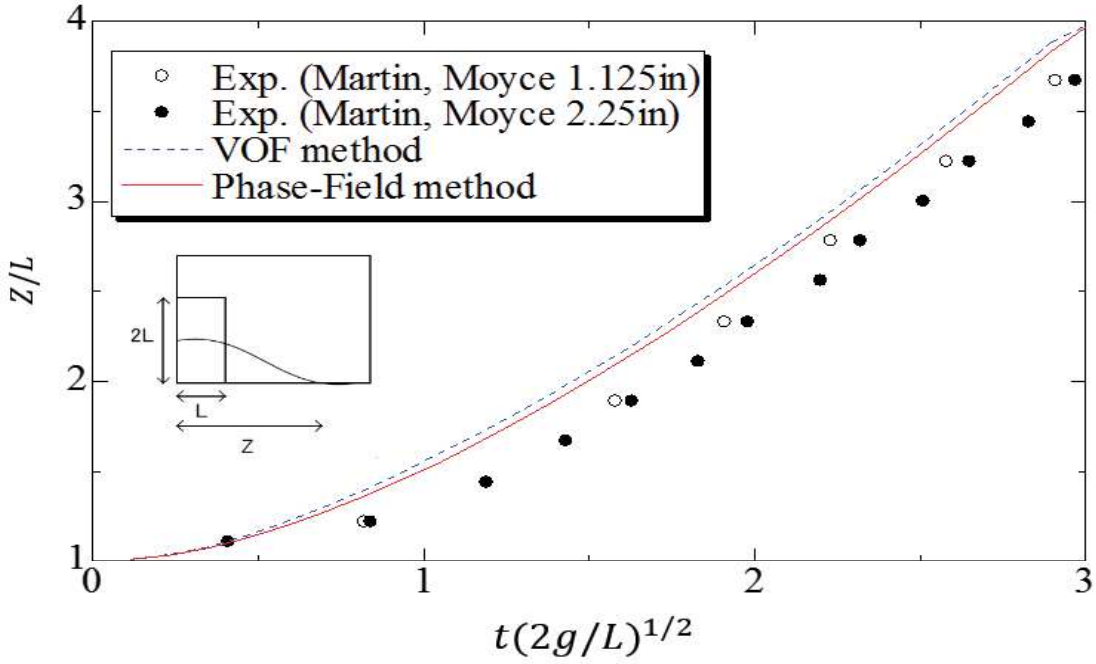

Figure 3.17 **Time evolution of leading-edge position**

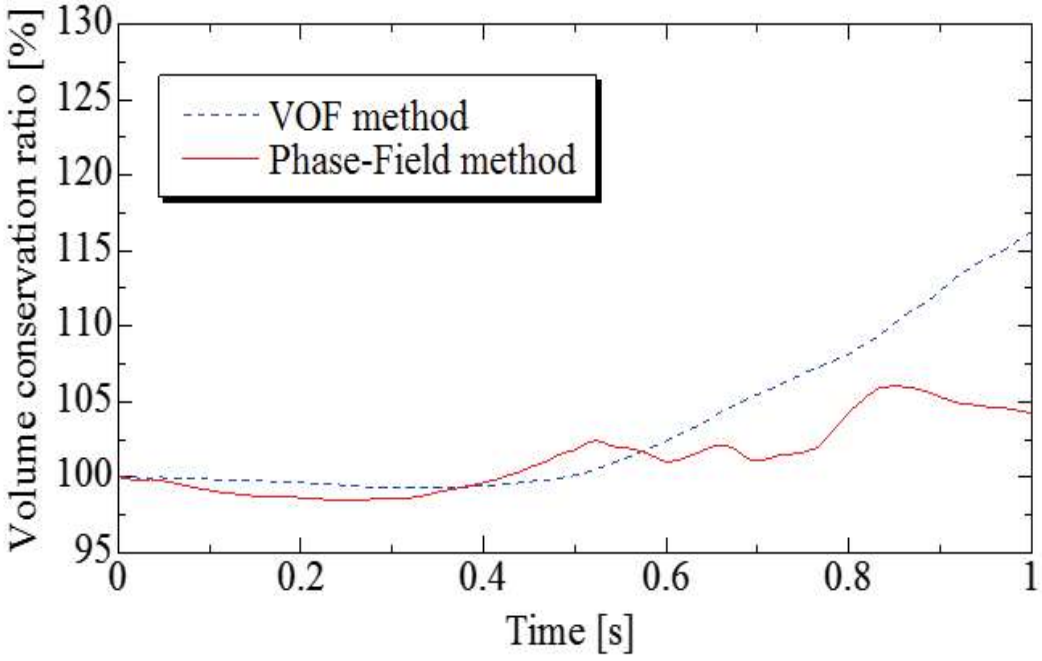

Figure 3.18 **Volume conservation ratio**

3.8.3 Dambreak With a Structure

To validate the 3D free surface flow analysis model using PFM, The dambreak with a structure problem [78] shown in **Figure 3.19** is simulated, and a comparison between the PFM and the VOF method is made. For the initial conditions, a water column is set on the left side of a rectangular aquarium, then release flow freely instantaneously just as the same as the hydraulic experiment did. The density and viscosity coefficient of water and air are set as, ρ_l=998.0kg/m^3, ρ_g=1.205kg/m^3, μ_l=1.01$\times$10^{-3}Pa$\cdot$s, and μ_g=1.81$\times$10^{-5}Pa$\cdot$s. For the computational conditions, $a_\delta = 3.0$, and $\gamma = 0.0005$. The computational mesh is showed in **Figure 3.20**, the minimum width is 0.005m, the number of nodes is 998,071 and the number of elements is 5,757,462. The time increment is set to be 0.001s and the slip condition is applied.

The surface profiles at $t = 1.50s$ are shown in **Figure 3.21**, we can see from the free surface, the PFM keep the surface more stable than the VOF. **Figure 3.22** shows the time history of the drag force acting in the x direction of the structure. From the figure, we can see the maximum drag force of the analysis results are in quite good agreement with the experimental result, though all the analysis results are moving faster to the structure. We can also see that for the drag force caused by the reflected wave, the PFM do better job than the VOF. And the PFM using the volume correction method [79] gives the best result. The mass conservation ratio is shown in **Figure 3.23**, we can see the PFM conserve the mass better than the VOF by using the same discretization methods. One of the reason for why the mass is not satisfied may due to overshoot and undershoot.

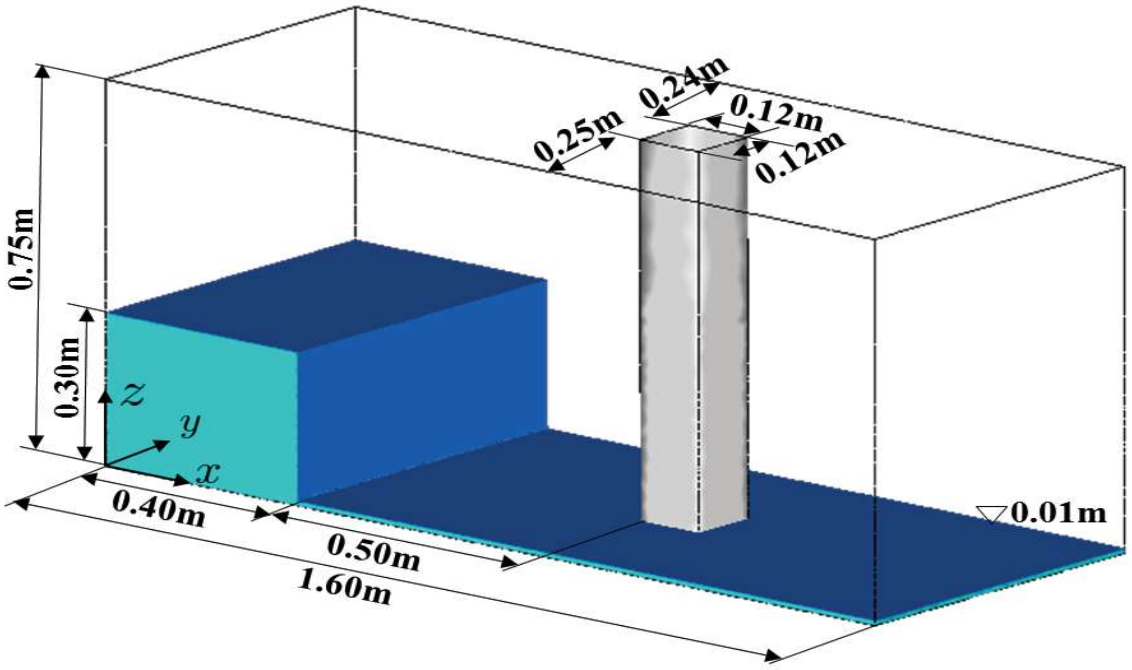

Figure 3.19 **Computational model**

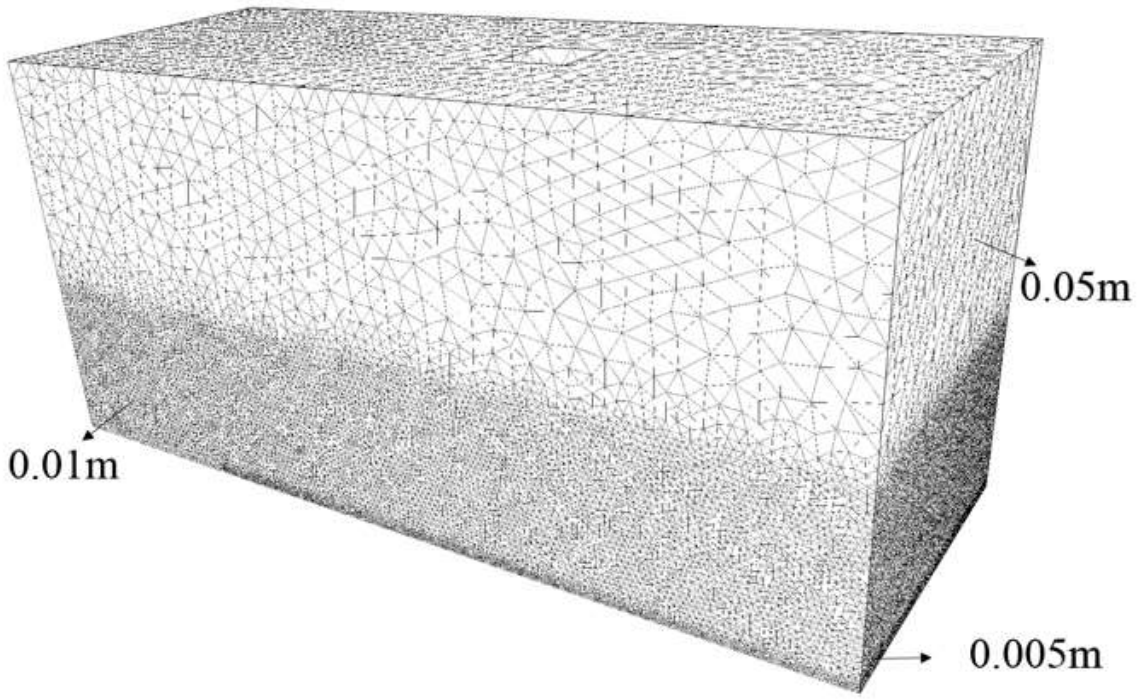

Figure 3.20 **Computational mesh**

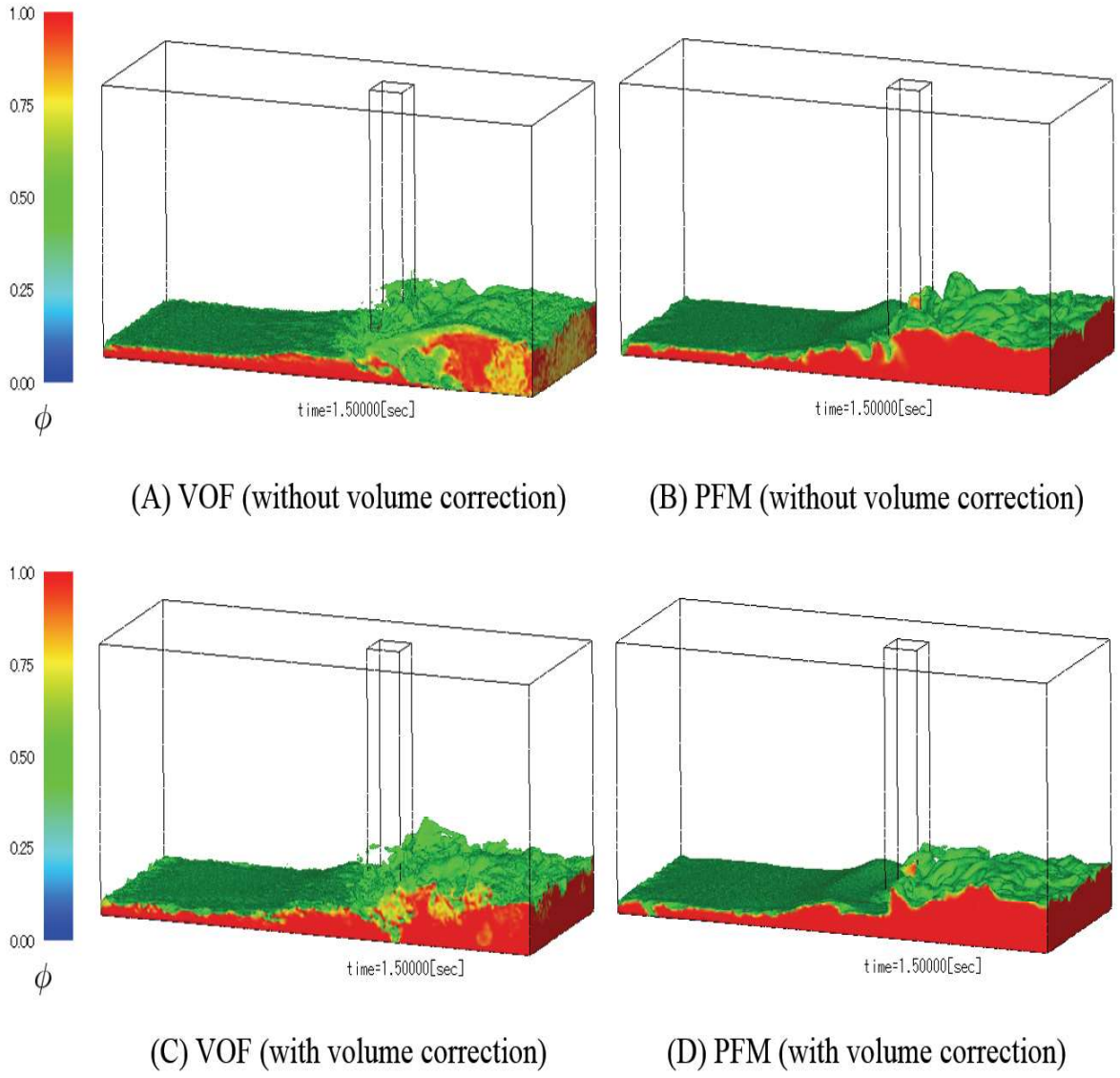

Figure 3.21 **Comparision of free surface at $t = 1.50$s**

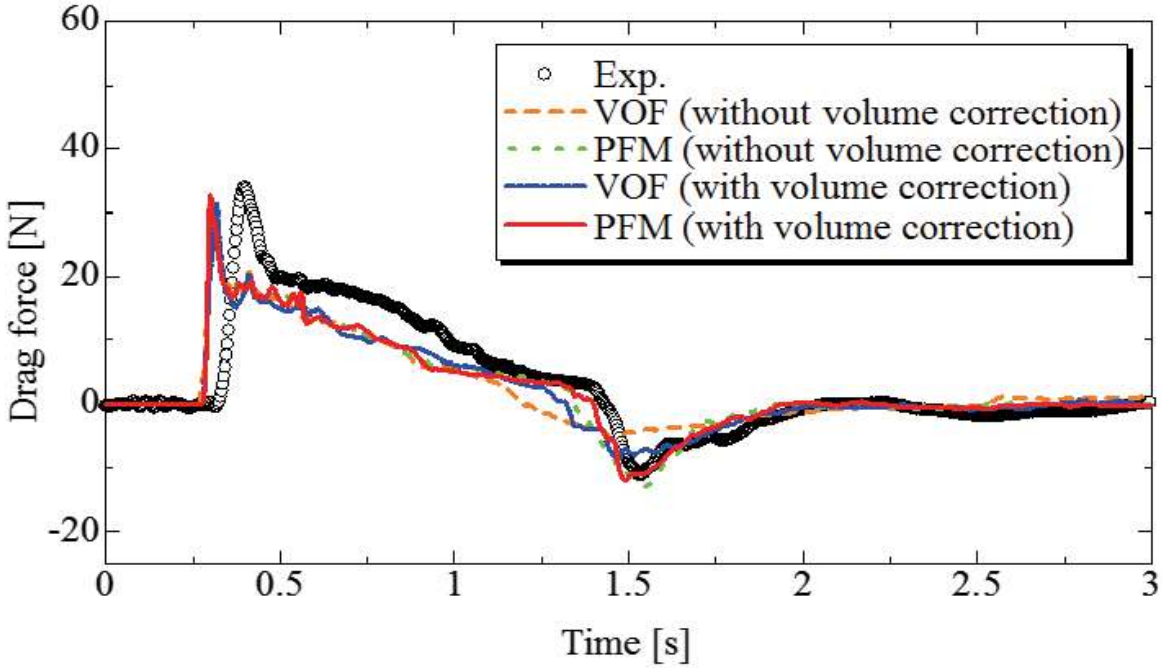

Figure 3.22 **Time history of force acting on the structure (x direction)**

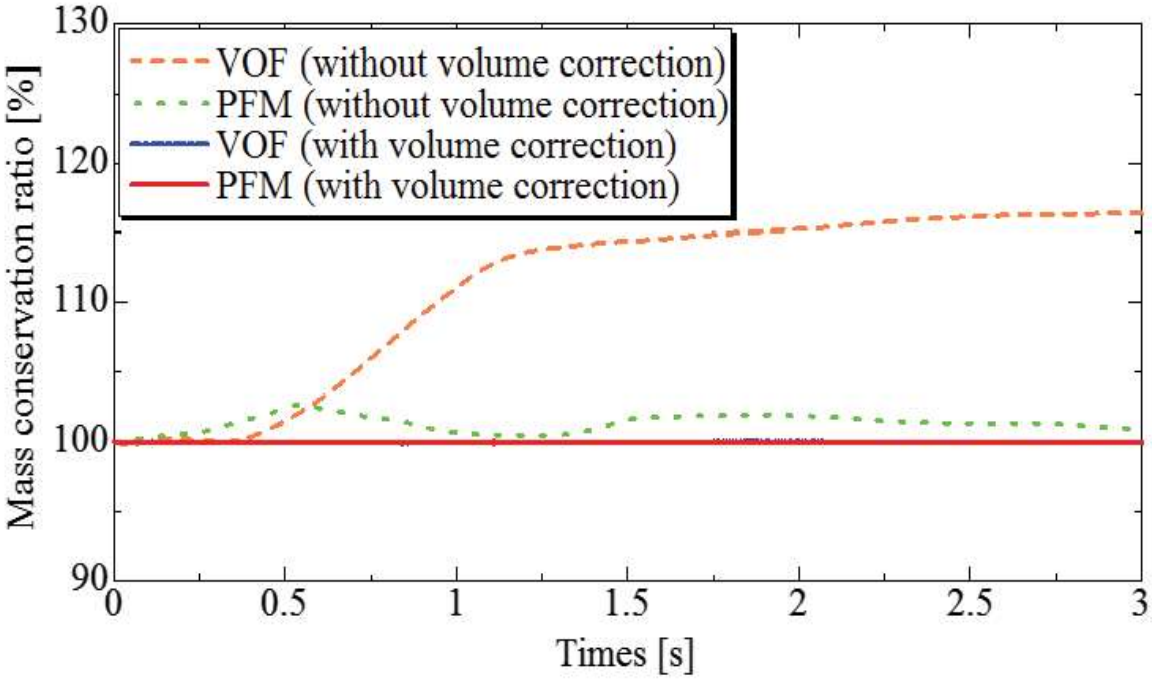

Figure 3.23 **Mass conservation ratio**

3.9 Chapter Summary

In this chapter, the PFM using the Allen-Cahn equation has been introduced, and the discretization of the Allen-Cahn equation using the stabilized finite element method has been presented. By comparison to the VOF method based on the advection equation, the following remarks can be concluded:

- From the rotating cylinder problem, the PFM can keep the interface for the two-phase flow and reduce the overshoot and undershoot. The interface width for PFM can be chosen as 2 or 3 times of the representative length of element. The interface energy with a large value may result in the shrink deformation.
- The PFM conserves the mass better than the VOF method by using the same finite element method.
- The drag force computed by the PFM is in a good agreement with the experimental result.

From the above remarks, the effectiveness of the present 3D analysis models using the PFM has been confirmed.